

On the Stability of Charge-Pump Phase-Locked Loops

Aliakbar Hodayoun, *Member, IEEE*, and Behzad Razavi, *Fellow, IEEE*

Abstract—This paper employs a time-variant model to determine the exact small-signal loop transmission of second-order charge-pump phase-locked loops. The model predicts that a loop bandwidth of close to half the input frequency can be achieved. The large-signal behavior is also analyzed and two modes of oscillation are identified. The results are confirmed by means of circuit simulations.

Index Terms—Harmonic balance, linear time-variant, phase margin, PLL model, PLLs, sampling, stability, wideband.

I. INTRODUCTION

TYPE-II phased locked loops (PLLs) incorporating charge pumps (CPs) find wide application in frequency synthesis and timing. In order to suppress the voltage-controlled oscillator (VCO) phase noise, it is desirable to maximize the bandwidth of such PLLs, but at the risk of instability.

Prior PLL stability studies can be divided into two broad categories. 1) Those dealing with loops that employ a mixer-type phase detector (PD) along with a continuous-time (CT) filter, for example, [1]–[9]; these PLLs do not perform sampling in the time domain and are not the focus of our paper. 2) Those involving loops that incorporate sampling before the loop filter, with either a mixer-type PD [9]–[13] or a phase/frequency detector (PFD) along with a charge pump [14]–[21]. One analysis approach in the latter group has been to model the sampling mechanism as a zero-order hold (ZOH), thereby obtaining the loop transmission in the s - and/or z -domains. We compare some of these papers' results with our findings in Section V. An important observation made in [18] is that charge-pump PLLs must be viewed as time-variant systems.

In this paper, we utilize a linear time-variant (LTV) model of the PFD and CP to propose an alternative analysis that provides new insights into the behavior of CP PLLs and shows that the loop bandwidth can approach one-half of the input frequency while maintaining stability. The theoretical findings are verified through circuit simulations of the standard PLL topology using VerilogA models in Cadence Spectre.

Manuscript received August 23, 2015; revised December 13, 2015 and January 24, 2016; accepted February 3, 2016. Date of publication May 25, 2016; date of current version June 15, 2016. This research was supported by Realtek Semiconductor. This paper was recommended by Associate Editor F. Bizzari.

The authors are with the Electrical Engineering Department, University of California at Los Angeles, Los Angeles, CA 90095-1594 USA (e-mail: hodayoun@g.ucla.edu; razavi@ee.ucla.edu).

Color versions of one or more of the figures in this paper are available online at <http://ieeexplore.ieee.org>.

Digital Object Identifier 10.1109/TCSI.2016.2537823

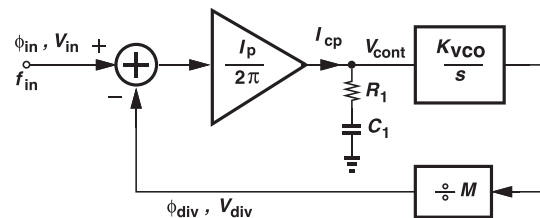


Fig. 1. LTI model of second-order charge-pump PLL.

Section II describes inconsistencies arising from the linear, time-invariant (LTI) model and Section III presents the proposed PFD/CP model. Section IV computes the loop transmission for small phase errors, and Section V determines the small signal stability bounds of second-order loop and prescribes a design procedure for a desired phase margin. Section VI analyzes the large-signal stability of the loop. Section VII deals with the stability of third-order loops.

II. GENERAL CONSIDERATIONS

Fig. 1 shows the conventional LTI model for a second-order charge-pump PLL. Commonly used by PLL designers [21]–[23], this phase-domain model gives a loop transmission equal to

$$T(s) = \frac{I_p}{2\pi} \cdot \frac{R_1 C_1 s + 1}{C_1 s} \cdot \frac{K_{VCO}}{M s} \quad (1)$$

where I_p is the charge pump current, R_1 and C_1 the loop filter components, K_{VCO} the gain of the VCO, and M the feedback divider ratio.¹ Due to its LTI nature, the model disregards sampling in the loop. Plotted in Fig. 2(a), the magnitude and phase of T exhibit two properties: $|T|$ monotonically drops to arbitrarily low values as ω increases, and $\angle T$ has only one deflection, from -180° toward -90° . A third property can be seen from the Nyquist plot of Fig. 2(b), namely, that the loop is stable. Note that the T contour reaches the origin at an angle of -90° as $\omega \rightarrow +\infty$. As described in Section IV, all of these three predictions are incorrect.

An intuitive perspective readily reveals why $|T(j\omega)|$ cannot monotonically fall. Consider a closed-loop configuration where the input contains phase modulation, $V_{in}(t) = V_1 \cos(\omega_{in}t + \alpha \cos \omega_m t)$. If ω_m is very low, the loop gain is extremely large and the phase error between the input and the output

¹This expression assumes a closed-loop transfer function of the form $G/(1+T)$, i.e., it does not contain the negative sign due to negative feedback around the loop.

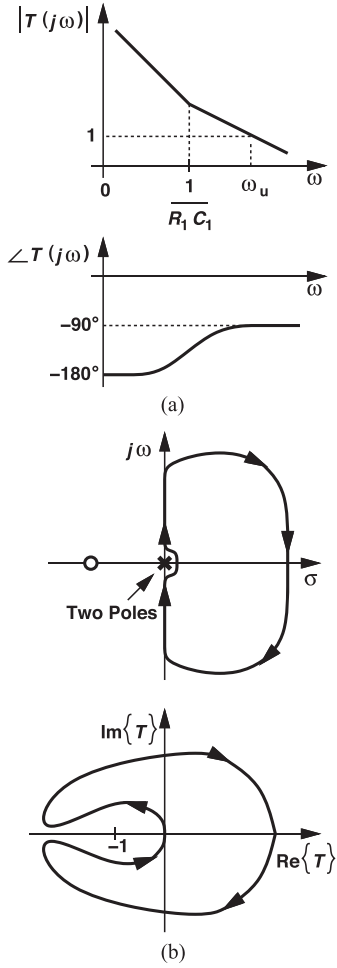


Fig. 2. (a) Bode and (b) Nyquist plots for the LTI model of a second-order charge-pump PLL.

vanishingly small. But suppose we choose $\omega_m = \omega_{in}$. Now, we recognize that $V_{in}(t) = V_1 \cos(\omega_{in}t + \alpha \cos \omega_{in}t)$ is *periodic* with a period of $T_{in} = 2\pi/\omega_{in}$, as if the input were not modulated at all. In this case, too, the phase error is zero because the PLL cannot distinguish between this input and an unmodulated input, implying that the loop gain must be *infinite*. Since this scenario repeats at all harmonics of ω_{in} , we predict that $|T(j\omega)|$ varies from infinity to a low value and back to infinity for each frequency span of $[n\omega_{in}(n+1)\omega_{in}]$.

III. PROPOSED PFD/CP MODEL

The LTI model of Fig. 1 assumes that the PFD/CP combination continuously subtracts the phase and applies the result to the VCO. In reality, however, the PFD/CP circuit produces current pulses only on the rising or falling edges of the reference input. For example, if in Fig. 1, $\Phi_{in} - \Phi_{div}(t) = \alpha \cos \omega_m t$, then the current pulses appear as shown in Fig. 3(a). If $\alpha \ll 1$ rad, then the width of these pulses is much less than T_{in} , allowing approximation of $I_{cp}(t)$ by impulses [Fig. 3(b)]. The subtractor in the conventional model must therefore be followed by multiplication by impulses [Fig. 3(c)], which is equivalent to ideal sampling.

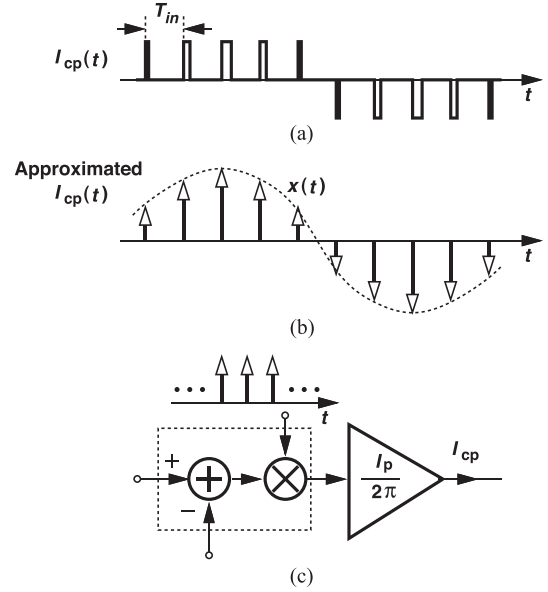


Fig. 3. (a) Charge pump pulses, (b) their impulse train approximation in response to a single-tone phase modulation at the PFD input, and (c) proposed PFD/CP model.

IV. LOOP TRANSMISSION COMPUTATION

As the first step in our stability analysis, we wish to determine the loop transmission of a charge-pump PLL using our proposed PFD/CP model.

A. Qualitative Analysis

In order to examine the loop transmission, we break the feedback path as shown in Fig. 4(a). We perturb the VCO by a sinusoid and seek the resulting response in V_{LPPF} . We call the perturbation the “excitation” and the response the “output.” To ensure that the VCO continues to operate at its original frequency, ω_0 , we choose V_{test} to include a proper dc component, V_{dc} , and a sinusoid:

$$V_{test}(t) = V_{dc} - V_0 \sin \omega_m t \quad (2)$$

where V_0 is assumed small (so that $V_0 K_{VCO}/\omega_m \ll 1$ rad). Upon traveling through the VCO and the divider, the signal emerges as

$$V_{div} = A \cos \left(\frac{\omega_0}{M} t + \frac{V_0 K_{VCO}}{M \omega_m} \cos \omega_m t \right) \quad (3)$$

yielding a phase error of $(V_0 K_{VCO}/M \omega_m) \cos \omega_m t$. This error is now sampled at a rate of f_{in} , producing the spectrum shown in Fig. 4(b), where $f_m = \omega_m/(2\pi)$. We note that the result contains impulse pairs at $\pm f_m, \pm f_{in} \pm f_m, \pm 2f_{in} \pm f_m$, etc. This spectrum is then scaled by $I_p/(2\pi)$ and shaped by the loop filter, producing V_{LPPF} .

The transfer function of interest is that relating the LPPF output components to the excitation $-V_0 \sin \omega_m t$. In fact, considering only the $\pm f_m$ components leads to a loop transmission of $[I_p/(2\pi)](K_{VCO}/s)Z_{LPPF}(s)$, as obtained from the standard continuous-time model. It is the *additional* output frequencies that alter the behavior of the loop.

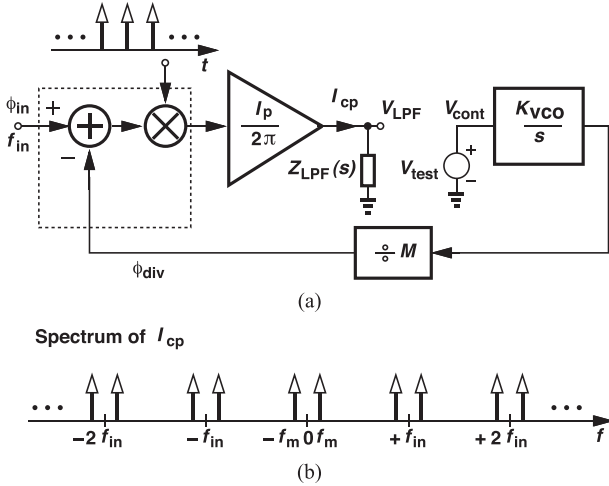


Fig. 4. (a) Open-loop PLL model, and (b) response to a modulated sinusoid on the VCO control voltage.

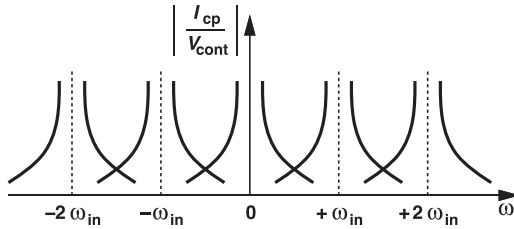


Fig. 5. Open-loop transfer function from the VCO control voltage to the charge pump current.

The foregoing analysis reveals that our choice of V_{test} is incomplete: if the feedback is restored, the frequency components around $\pm n f_{in}$, $n \neq 0$, also circulate around the loop, experiencing aliasing in the PFD/CP circuit and possibly contributing to the components of interest at $\pm f_m$. We must therefore predict all of the circulating frequencies in a manner similar to harmonic balance analysis.

It is possible to view the VCO/divider/PFD/CP cascade as a translational circuit. That is, the VCO/divider transfer function, $K_{VCO}/(jM\omega)$ is translated to the harmonics of ω_{in} (Fig. 5), with the tails of the responses at $\pm k\omega_{in}$, $k \neq 0$, contributing to the main transfer function around $\omega = 0$ and degrading the stability. However, this open-loop transmission faces difficulties because of the time-variant nature of the system. Unlike LTI systems, the *order* of functions in an LTV cascade cannot be changed, e.g., low-pass filtering followed by mixing is not the same as mixing followed by low-pass filtering. For this reason, the PLL exhibits different loop transmissions if broken at different points! We therefore analyze the PLL in closed loop form.

B. Quantitative Analysis

While intuitively appealing, the foregoing open-loop approach does not easily lend itself to harmonic balance analysis. In order to determine the loop transmission, we instead postulate that, if the *closed-loop* transfer function of the PLL is derived as $G/(1+T)$, then T is the desired expression. To

this end, we apply to the closed-loop PLL an input containing a small phase modulation, $V_{in}(t) = V_1 \cos(\omega_{in}t + \alpha \cos \omega_m t)$, where $\alpha \ll 1$ rad, and follow the signal and its sampled replicas around the loop, assuming that the PLL remains locked. (We deal with the large-signal behavior of the PLL in Section VI.) Note that any signal within the loop can be viewed as the “output” for this calculation.

Before delving into the analysis, we make three observations. First, due to the impulse sampling action, the spectrum of the charge pump output current contains impulses at $\pm n f_{in} \pm f_m$.

Second, even after traveling around the loop and returning through the PFD/CP cascade, the above components cannot generate frequencies other than $\pm n f_{in} \pm f_m$ because sampling at a rate of f_{in} simply shifts the spectrum up and down by integer multiples of f_{in} .

Third, in the steady state, the impulses at $\pm n f_{in} \pm f_m$ at the CP output have *equal* magnitudes because each arises from the *same* components (infinite in number) that return through the feedback divider and experience impulse sampling. For example, an impulse at $+7f_{in} + f_m$ is created by a feedback component at $8f_{in} + f_m$ after it is shifted to the left by f_{in} , or by a component at $9f_{in} + f_m$ after it is shifted to the left by $2f_{in}$, etc., and also by any other component, $k f_{in} + f_m$, after it is shifted by $(7-k)f_{in}$.

The last observation paves the way for our harmonic balance analysis. If the CP output frequency components have equal magnitudes, then upon traveling through the VCO and the divider, mixing with the input, and experiencing impulse sampling, they must still yield equal magnitudes.

Fig. 6 summarizes the spectra at various points around the loop. As shown in Appendix A, we view $\beta/\alpha = I_{cp}(s)/\Phi_{in}(s)$ as the closed-loop transfer function and there-from obtain the loop transmission as

$$T(j\omega) = \frac{I_p K_{VCO}}{2\pi M} \sum_{n=-\infty}^{\infty} \frac{Z_{LPF}[j(n\omega_{in} + \omega)]}{j(n\omega_{in} + \omega)}. \quad (4)$$

This equation confers a great deal of insight into the behavior of PLLs and forms the foundation of our analysis. Since (4) assumes small-signal phase perturbations (for the impulse approximation in Fig. 3 to hold), we analyze the large-signal behavior separately. Before considering a specific loop, we offer a conjecture. The phase margin of the time-variant PLL is smaller than that of the continuous-time approximation because the folding of the higher harmonics both *raises* the real part of $T(j\omega)$ and *lowers* the imaginary part. This conjecture is proved below.

V. SMALL-SIGNAL ANALYSIS OF SECOND-ORDER LOOP

A. Stability Bounds

As mentioned in Section III, for small phase errors in a PLL, the charge pump output can be approximated by a train of impulses, leading to a linear system. For a second-order PLL, we assume a loop filter impedance $Z_{LPF}(j\omega) = R_1 + 1/(jC_1\omega)$. Equation (4) thus yields

$$T(j\omega) = -\frac{I_p K_{VCO}}{2\pi M C_1} \sum_{n=-\infty}^{\infty} \frac{1 + jR_1 C_1 (n\omega_{in} + \omega)}{(n\omega_{in} + \omega)^2}. \quad (5)$$

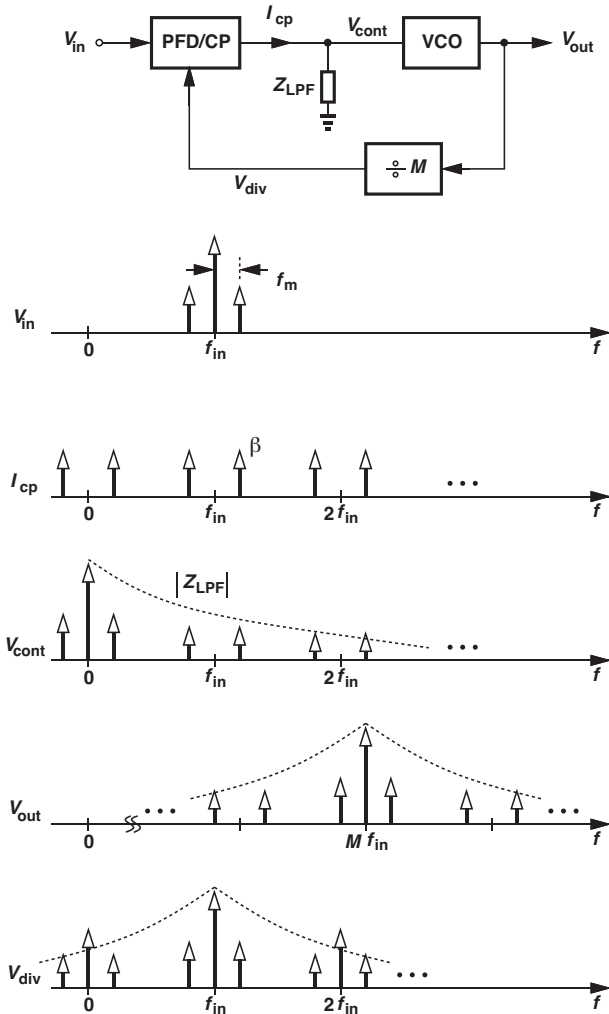


Fig. 6. Spectra at various points in response to a phase-modulated sinusoid at the input of a closed-loop PLL.

We examine this loop transmission from different viewpoints so as to gain insight into the stability behavior. Let us first write the real and imaginary parts of $T(j\omega)$ as

$$\operatorname{Re}\{T(j\omega)\} = -\frac{I_p K_{VCO}}{2\pi M C_1} \sum_{n=-\infty}^{\infty} \frac{1}{(n\omega_{in} + \omega)^2} \quad (6)$$

$$= -\frac{I_p K_{VCO}}{2M C_1 \omega_{in}^2} \frac{\pi}{\sin^2\left(\frac{\pi\omega}{\omega_{in}}\right)}. \quad (7)$$

$$\operatorname{Im}\{T(j\omega_u)\} = -\frac{I_p K_{VCO} R_1}{2\pi M} \sum_{n=-\infty}^{\infty} \frac{1}{(n\omega_{in} + \omega)}$$

$$= -\frac{I_p K_{VCO} R_1}{2\pi M} \left(\frac{1}{\omega} + \sum_{n=1}^{\infty} \frac{2\omega}{\omega^2 - n^2 \omega_{in}^2} \right) \quad (8)$$

$$= -\frac{I_p K_{VCO} R_1}{2M \omega_{in}} \cot \frac{\pi\omega}{\omega_{in}}. \quad (9)$$

Note that the former is a function of I_p/C_1 and the latter, $I_p R_1$.

Fig. 7 plots $-\operatorname{Re}\{T(j\omega)\}$ and $-\operatorname{Im}\{T(j\omega)\}$ as a function of ω , revealing two interesting properties: 1) $-\operatorname{Re}\{T\}$ reaches

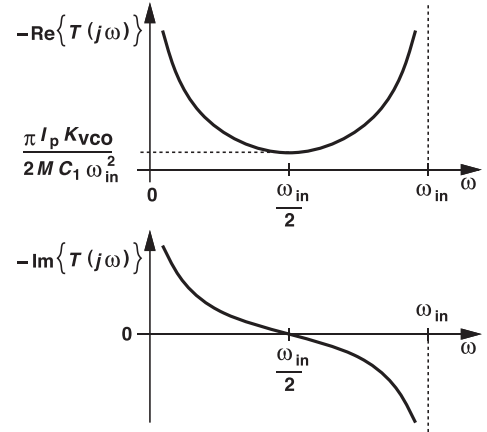


Fig. 7. Real and imaginary part of $-T(j\omega)$ for the second-order loop.

a minimum at $\omega = \omega_{in}/2$ (and its higher odd harmonics) and goes to $+\infty$ at $\omega = 0, \omega_{in}, 2\omega_{in}$, etc.; 2) $-\operatorname{Im}\{T\}$ falls to zero at $\omega = \omega_{in}/2$, yielding $\angle T(j\omega_{in}/2) = 180^\circ$, and goes to $+\infty$ at $\omega = 0$ and to $-\infty$ at $\omega = \omega_{in}, 2\omega_{in}$, etc. We also observe that, as more harmonics are considered in (6) and (8) (i.e., as n increases), (6) rises monotonically and (8) becomes more negative monotonically, *degrading* the phase margin.

The above plots provide the stability condition if we note that $|T(j\omega_{in}/2)|^2 = \operatorname{Re}^2\{T(j\omega_{in}/2)\} + \operatorname{Im}^2\{T(j\omega_{in}/2)\} = \operatorname{Re}^2\{T(j\omega_{in}/2)\}$, concluding that $\operatorname{Re}\{T(j\omega_{in}/2)\}$ must be less than unity because the phase crosses -180° at this frequency. This means that the unity-gain bandwidth of T , ω_u , cannot exceed $\omega_{in}/2$. It follows from (7) that:

$$\frac{\pi I_p K_{VCO}}{2M C_1 \omega_{in}^2} < 1 \quad (10)$$

and hence

$$C_1 > \frac{\pi I_p K_{VCO}}{2M \omega_{in}^2} \equiv C_{\text{stable}}. \quad (11)$$

We consider C_{stable} as the lower bound on C_1 for stability.

In order to contrast the loop behavior formulated by our analysis to that in Fig. 2, we utilize (7) and (9) to express $|T|$ and $\angle T$, respectively, as:

$$|T|^2 = \frac{I_p^2 K_{VCO}^2}{4M^2 C_1^2 \omega_{in}^4} \frac{\pi^2 + \frac{R_1^2 C_1^2 \omega_{in}^2}{4} \sin^2 \frac{2\pi\omega}{\omega_{in}}}{\sin^4 \frac{\pi\omega}{\omega_{in}}} \quad (12)$$

$$\angle T = -180^\circ + \tan^{-1} \left(\frac{R_1 C_1 \omega_{in}}{2\pi} \sin \frac{2\pi\omega}{\omega_{in}} \right). \quad (13)$$

Depicted in Fig. 8(a) are sketches of $|T|$ and $\angle T$, demonstrating the nonmonotonic behavior of the former and the phase deflections in the latter. To construct the Nyquist plot, we assume that T follows the LTI behavior of Fig. 2(b) for low values of ω . As ω increases, $|T|$ falls to a finite value, $\pi I_p K_{VCO}/(2M C_1 \omega_{in}^2)$, while $\angle T$ does not reach -90° . As shown in Fig. 8(b), the T contour crosses the real axis at a negative value for $\omega = \omega_{in}/2$, suggesting instability if this point is to the left of $(-1, 0)$ and leading to the condition expressed by (10).²

²It can be proved that T has no zeros in the right half plane: if $V_{\text{test}} = e^{st}$ and $s = \sigma + j\omega$ in Fig. 4(a), then $V_{L\text{LPF}}$ cannot be zero for $\sigma > 0$.

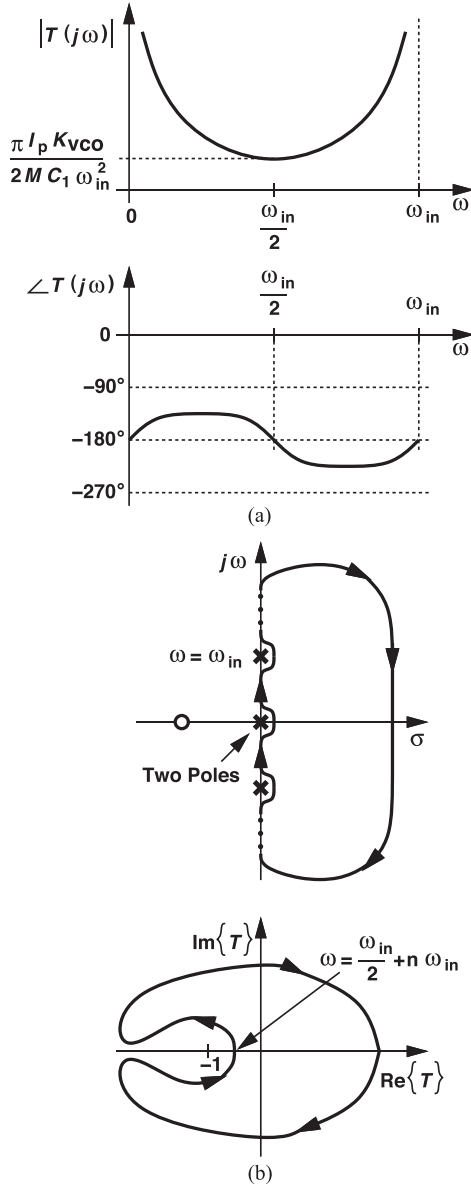


Fig. 8. (a) Bode and (b) Nyquist plots for the proposed model of a second-order charge-pump PLL.

In summary, our results prove that the Nyquist contour of a second-order PLL encircles the point $(-1, 0)$ if the minimum value of $|T|$ in Fig. 8 exceeds 1, i.e., if the loop bandwidth is greater than $\omega_{in}/2$. To our knowledge, prior work has not recognized these properties.

We remark that [14, Eq. (14)] can be rearranged to read

$$C_1 = \frac{\pi I_p K_{VCO}}{M \omega_{in} (2\omega_{in} - R_1 I_p K_{VCO}/M)} \quad (14)$$

which agrees with (11) only if $R_1 I_p K_{VCO}/M \ll 2\omega_{in}$. Also, (14) implies that $R_1 I_p K_{VCO}/M$ must remain less than $2\omega_{in}$, whereas we show below that a stable loop can be constructed that violates this condition. That is, (11) appears to be a more accurate bound on the stability.

We can also compare our results to that obtained by [20] using a zero-order-hold model and z-transform analysis. Equation

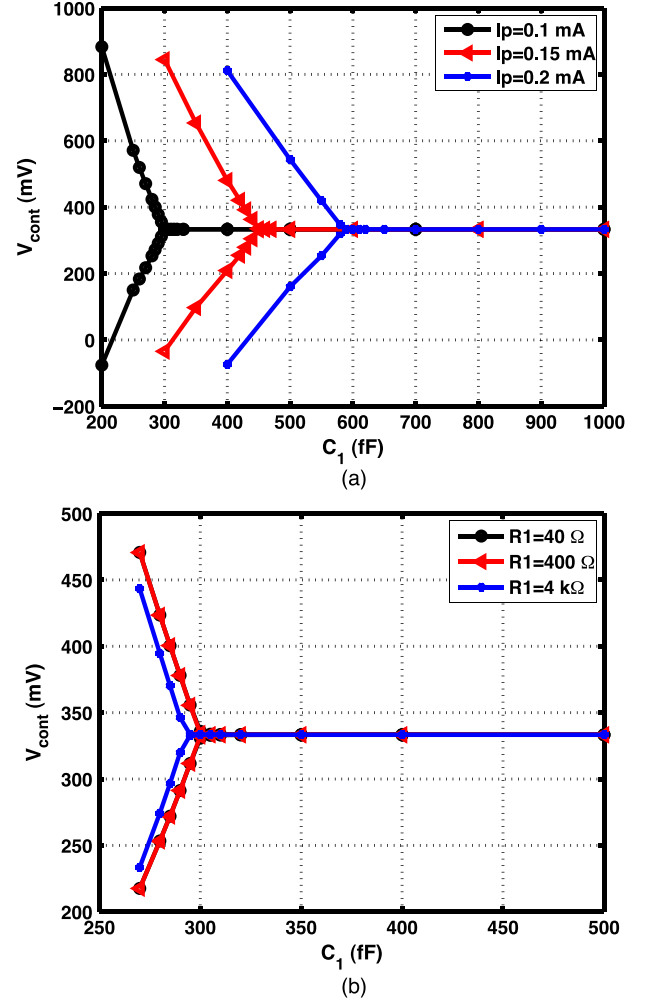


Fig. 9. Steady-state V_{cont} amplitude as a function of C_1 when PLL is initially locked for $\omega_{in} = 2\pi \times (125 \text{ MHz})$, $K_{VCO} = 2\pi \times (1.5 \text{ GHz})$, $M = 8$, and (a) $R_1 = 2 \text{ k}\Omega$, and (b) $I_p = 0.1 \text{ mA}$.

(3.42) in [20] can be rewritten as

$$\omega_{in} \geq \frac{R_1 I_p K_{VCO}}{2M} \quad (15)$$

a condition independent of C_1 . As shown below, with $\omega_{in} = 2\pi \times (125 \text{ MHz})$, $R_1 \approx 31 \text{ k}\Omega$, $I_p = 0.1 \text{ mA}$, $K_{VCO} = 2\pi \times (1.5 \text{ GHz/V})$, and $M = 8$, the actual loop is stable but the right side of (15) reaches $2\pi \times (291 \text{ MHz})$. Equation (15) therefore appears to fail in at least some cases.

In order to verify our small-signal derivations, we have run extensive simulations while incrementing C_1 in small steps. In this case, the loop is initially locked and then subject to a small perturbation to see whether it remains stable. Plotted in Fig. 9(a) is a family of curves of V_{cont} vs. C_1 with $\pi I_p K_{VCO}/(M \omega_{in}^2)$ as a parameter. Here, the diverging values of V_{cont} indicate loop instability. As expected, once C_1 falls below $\pi I_p K_{VCO}/(2M \omega_{in}^2)$, the loop becomes unstable. The critical values of C_1 observed in these simulations agree with (11).

The above simulations have also been repeated with R_1 as a parameter, and the results are depicted in Fig. 9(b). Again, the simulations match (11).

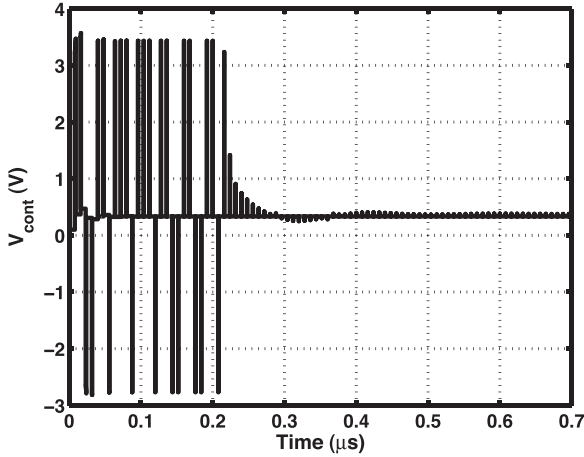


Fig. 10. PLL transient behavior for a phase margin of 50° simulated by Cadence Spectre using a reltol of $1e-7$.

B. Design for a Given Phase Margin

The stability bound expressed by (11) yields a zero phase margin (PM). For a desired PM of θ , we set $\angle T(j\omega_u) = 180^\circ - \theta$, where ω_u denotes the unity-gain bandwidth of $|T(j\omega)|$. It follows that:

$$\operatorname{Re}\{T(j\omega_u)\} = \cos \theta \quad (16)$$

$$\operatorname{Im}\{T(j\omega_u)\} = \sin \theta. \quad (17)$$

The former gives, along with (7), the necessary value of C_1 :

$$\begin{aligned} C_1 &= \frac{\pi I_p K_{VCO}}{2M\omega_{in}^2 \cos \theta \sin^2\left(\frac{\pi\omega_u}{\omega_{in}}\right)} \\ &= \frac{1}{\cos \theta \sin^2\left(\frac{\pi\omega_u}{\omega_{in}}\right)} C_{stable}. \end{aligned} \quad (18)$$

Similarly, (9) and (17) lead to

$$R_1 = \frac{2M\omega_{in} \sin \theta \tan\left(\frac{\pi\omega_u}{\omega_{in}}\right)}{I_p K_{VCO}}. \quad (19)$$

The key observation here is that ω_u is still an independent variable and can be chosen close to $\omega_{in}/2$ for any desired phase margin—albeit at the cost of an impractically large R_1 as ω_u approaches $\omega_{in}/2$.

As an example, let us select $K_{VCO} = 2\pi \times (1.5 \text{ GHz/V})$, $\omega_{in} = 2\pi \times (125 \text{ MHz})$, $M = 8$, and $I_p = 0.1 \text{ mA}$. To obtain $\omega_u = 0.4\omega_{in}$ and $\theta = 50^\circ$, we calculate $C_1 \approx 520 \text{ fF}$ from (18) and $R_1 \approx 31 \text{ k}\Omega$ from (19). Depicted in Fig. 10 is the transient response of such a loop using an ideal charge pump, where the oscillator control voltage, V_{cont} is plotted versus time. The absence of a second capacitor allows large jumps equal to $I_p R_1$ in V_{cont} . As the PLL approaches lock, the amplitude of the voltage jumps decreases, but does not fully disappear due to the discrete nature of the simulator. We observe a stable system even if V_{cont} begins with a large error. Interestingly, the LTI model predicts a phase margin of 88° for such a loop whereas (14) implies instability (because $R_1 I_p K_{VCO}/M > 2\omega_{in}$), neither a reasonable approximation of reality.

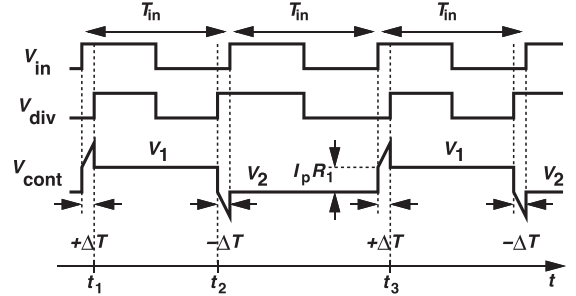


Fig. 11. Oscillatory behavior for the $f_{in}/2$ mode.

We conclude this section with one more observation. If $\omega_u \ll \omega_{in}/\pi$, then (18) and (19) reduce to their LTI counterparts

$$C_{1,LTI} = \frac{I_p K_{VCO}}{2\pi M \omega_u^2 \cos \theta} \quad (20)$$

$$R_{1,LTI} = \frac{2\pi M \omega_u \sin \theta}{I_p K_{VCO}}. \quad (21)$$

Even for the common rule of thumb $\omega_u \approx 0.1\omega_{in}$, the discrepancy between LTV and LTI values is less than 3%; our analysis therefore rigorously proves the accuracy of the LTI model when $\omega_u \approx 0.1\omega_{in}$.

VI. LARGE-SIGNAL ANALYSIS OF SECOND-ORDER LOOP

If the PLL transient begins with a large phase error, then the loop is nonlinear and must be analyzed as such. In this section, we identify two large-signal oscillation modes and determine the conditions for avoiding them.

The first mode is oscillation at a frequency equal to $f_{in}/2$, i.e., the oscillator control voltage, V_{cont} , toggles between two values in consecutive input cycles. Fig. 11 plots the steady-state waveforms that we expect to observe in this case for the PLL of Fig. 6. In one cycle, the loop incurs a phase error of ΔT between the input, V_{in} , and the feedback signal (the divider output), V_{div} , turning on the charge pump when V_{in} rises and creating a jump equal to $I_p R_1$ on V_{cont} . (In a second-order PLL, V_{cont} can jump instantaneously.) The CP charges the loop filter for ΔT seconds and then turns off, allowing V_{cont} to fall by $I_p R_1$ to a value V_1 . This voltage is so large that, after integration by the VCO for $T_{in} - \Delta T$ seconds, it produces a phase error of $-\Delta T$. Thus, the next cycle proceeds with opposite voltage changes. Note that the period of V_{div} toggles between $T_{in} - 2\Delta T$ and $T_{in} + 2\Delta T$, i.e., the phase of V_{div} is periodically modulated.

To formulate the loop behavior in this mode, we observe that V_{div} exhibits one complete cycle from t_1 to t_2 in Fig. 11. Thus if we integrate $K_{VCO} V_1$ from t_1 to t_2 and divide it by M , we should obtain 2π

$$\frac{K_{VCO} V_1 (T_{in} - 2\Delta T)}{M} = 2\pi \quad (22)$$

Similarly, integration from t_2 to t_3 yields

$$\frac{K_{VCO} V_2 T_{in}}{M} + K_{VCO} \frac{V_1 + V_2}{2M} 2\Delta T = 2\pi. \quad (23)$$

We also have

$$V_1 - V_2 = \frac{I_p \Delta T}{C_1}. \quad (24)$$

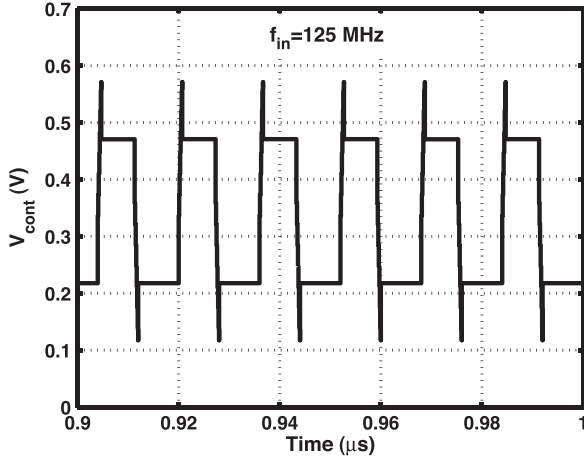


Fig. 12. Simulated $f_{in}/2$ mode of oscillation with $C_1 = 270 \text{ fF} < C_{stable} = 300 \text{ fF}$.

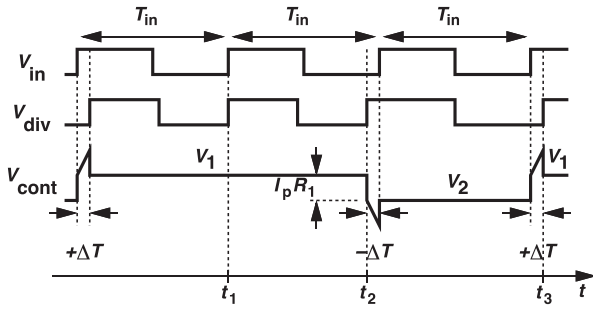


Fig. 13. Oscillatory behavior for the $f_{in}/3$ mode.

It follows that:

$$2\Delta T^2 + T_{in}\Delta T + \frac{8\pi C_1}{I_p K_{VCO}} - T_{in}^2 = 0. \quad (25)$$

To avoid oscillation, we must ensure that this equation does not have a real solution, i.e.,

$$C_1 > \frac{\pi I_p K_{VCO}}{2M\omega_{in}^2} = C_{stable}. \quad (26)$$

Interestingly, this result is the same as that obtained from the linear time-variant (small-signal) analysis. It is important to observe that the above derivations are independent of R_1 . To verify this result, we simulate the loop described in the previous section but select $C_1 < C_{stable}$, obtaining the transient response shown in Fig. 12. The oscillation occurs as predicted above.

The second mode of oscillation occurs at a frequency of $f_{in}/3$. As illustrated in Fig. 13, the divider output rising edge leads, coincides with, and lags that of the input over successive cycles. The period of V_{div} is equal to $T_{in} - \Delta T$ for two cycles and $T_{in} + 2\Delta T$ for one cycle, and the pattern is repeated. Since V_{div} exhibits one complete cycle from t_1 to t_2

$$\frac{K_{VCO}V_1(T_{in} - \Delta T)}{M} = 2\pi. \quad (27)$$

Similarly, integration from t_2 to t_3 gives

$$\frac{K_{VCO}V_2T_{in}}{M} + K_{VCO}\frac{V_1 + V_2}{2M}2\Delta T = 2\pi. \quad (28)$$

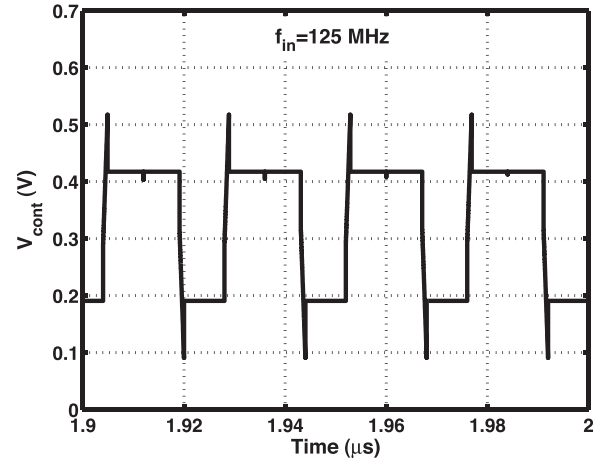


Fig. 14. Simulated $f_{in}/3$ mode of oscillation with $C_1 = 395 \text{ fF} < 4C_{stable}/3 = 400 \text{ fF}$.

We also have $V_1 - V_2 = I_p\Delta T/C_1$. Solving for ΔT yields

$$\Delta T = \sqrt{T_{in}^2 - \frac{6\pi C_1}{I_p K_{VCO}}}. \quad (29)$$

To avoid this mode, we must have

$$C_1 > \frac{2\pi I_p K_{VCO}}{3M\omega_{in}^2} = \frac{4}{3}C_{stable}. \quad (30)$$

This condition sets a tighter stability threshold than those derived above. Fig. 14 depicts the transient behavior if $C_{stable} < C_1 < (4/3)C_{stable}$. For $C_1 < C_{stable}$, the PLL can oscillate in either mode depending on the initial states (the initial frequency and phase of the VCO). Note that this mode, too, is independent of R_1 . Higher modes can be analyzed in a similar manner as described in Appendix B.

The tighter condition given by (30) prevails in a practical design. However, the condition stipulated by (11) also predicts the response of the loop to small perturbations in the locked condition, as illustrated in Fig. 9. The two results therefore prove useful to the analysis and design.

In order to verify our large-signal derivations, we repeat the simulations of Fig. 9 but this time with an arbitrary initial condition. Plotted in Fig. 15(a) is a family of curves of V_{cont} vs. C_1 with $\pi I_p K_{VCO}/(M\omega_{in}^2)$ as a parameter. As expected, once C_1 falls below $2\pi I_p K_{VCO}/(3M\omega_{in}^2)$, the loop becomes unstable. The critical values of C_1 observed in these simulations agree with (30).

The above simulations have also been repeated with R_1 as a parameter, and results are depicted in Fig. 15(b). Again, the simulations match (30).

VII. SMALL-SIGNAL ANALYSIS OF THIRD-ORDER LOOP

Actual charge pump PLLs incorporate a second capacitor, C_2 , in parallel with R_1 and C_1 in Fig. 1 so as to reduce the ripple on the VCO control voltage. In this case, the filter impedance $Z_{LPF}(j\omega)$ in Fig. 4 is expressed as

$$Z_{LPF}(j\omega) = \frac{1}{j(C_1 + C_2)\omega} \frac{1 + jR_1C_1\omega}{1 + jR_1C_{eq}\omega} \quad (31)$$

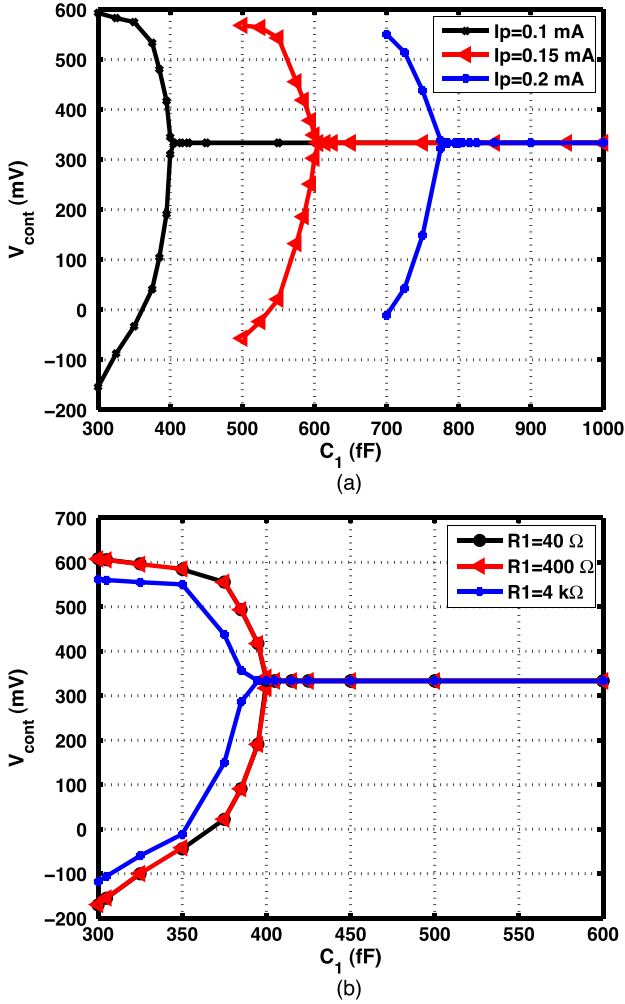


Fig. 15. Steady-state V_{cont} as a function of C_1 when PLL is initially far from lock for $\omega_{\text{in}} = 2\pi \times (125 \text{ MHz})$, $K_{\text{VCO}} = 2\pi \times (1.5 \text{ GHz})$, $M = 8$, and (a) $R_1 = 2 \text{ k}\Omega$, and (b) $I_p = 0.1 \text{ mA}$.

where C_{eq} is $C_1 C_2 / (C_1 + C_2)$. Since the new pole at $(-R_1 C_{\text{eq}})^{-1}$ is always higher than the zero, $(-R_1 C_1)^{-1}$, the continuous-time model predicts that the loop is still stable! Substituting (31) in (4), we obtain the loop transmission as

$$T(j\omega) = \frac{I_p K_{\text{VCO}}}{2\pi M (C_1 + C_2)} \times \sum_{n=-\infty}^{\infty} \frac{1 + R_1^2 C_1 C_{\text{eq}} (n\omega_{\text{in}} + \omega)^2 + j R_1 (C_1 - C_{\text{eq}}) (n\omega_{\text{in}} + \omega)}{(n\omega_{\text{in}} + \omega)^2 [1 + R_1^2 C_{\text{eq}}^2 (n\omega_{\text{in}} + \omega)^2]} \quad (32)$$

As with the second-order loop, inclusion of higher harmonics of ω_{in} makes the loop less stable. The imaginary part of $T(j\omega)$ vanishes at $\omega = \omega_{\text{in}}/2$, leading to a real part equal to

$$\text{Re} \left\{ T \left(j \frac{\omega_{\text{in}}}{2} \right) \right\} = \frac{\pi I_p K_{\text{VCO}}}{2M (C_1 + C_2) \omega_{\text{in}}^2} + \frac{I_p K_{\text{VCO}} R_1}{2M (1 + C_2/C_1)^2 \omega_{\text{in}}^2} \tanh \frac{\pi}{R_1 C_{\text{eq}} \omega_{\text{in}}} \quad (33)$$

This quantity must remain less than unity for the loop to be stable.

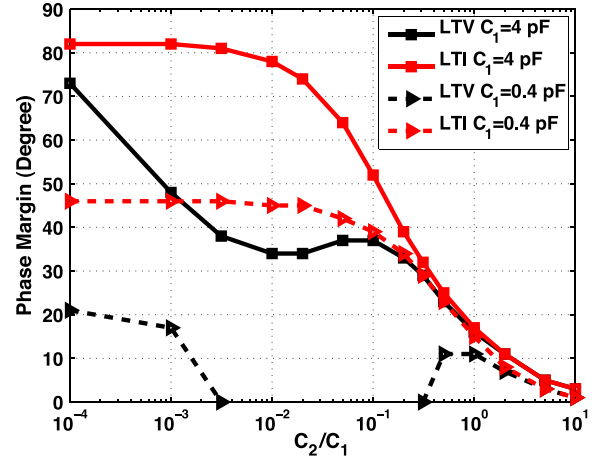


Fig. 16. Phase margin of third-order PLL as predicted by LTI and LTV models where $\omega_{\text{in}} = 2\pi \times (125 \text{ MHz})$, $K_{\text{VCO}} = 2\pi \times (1.5 \text{ GHz})$, $M = 8$, $I_p = 0.1 \text{ mA}$, and $R_1 = 10 \text{ k}\Omega$.

To develop insight, let us study the above result in two extreme cases. If $R_1 C_{\text{eq}} \omega_{\text{in}} \gg 1$, then $\tanh[\pi / (R_1 C_{\text{eq}} \omega_{\text{in}})] \approx \pi / (R_1 C_{\text{eq}} \omega_{\text{in}})$ and hence

$$\text{Re} \left\{ T \left(j \frac{\omega_{\text{in}}}{2} \right) \right\} \approx \frac{\pi I_p K_{\text{VCO}}}{2M C_2 \omega_{\text{in}}^2} \quad (34)$$

For loop stability, we must have

$$C_2 > \frac{\pi I_p K_{\text{VCO}}}{2M \omega_{\text{in}}^2} = C_{\text{stable}} \quad (35)$$

For example, if R_1 is very large, the loop filter reduces to C_2 , readily imposing this condition from (11). This case is unlikely to occur in practice because it is equivalent to $R_1 C_{\text{eq}} \gg 2\pi / T_{\text{in}} > 1 / T_{\text{in}}$, i.e., it assumes that charge sharing between C_2 and C_1 is not completed in one input cycle (after the charge pump turns off).

The second extreme case arises if $R_1 C_{\text{eq}} \omega_{\text{in}} \ll 1$, yielding $\tanh[\pi / (R_1 C_{\text{eq}} \omega_{\text{in}})] \approx 1$ and

$$\text{Re} \left\{ T \left(j \frac{\omega_{\text{in}}}{2} \right) \right\} \approx \frac{\pi I_p K_{\text{VCO}}}{2M (C_1 + C_2) \omega_{\text{in}}^2} \quad (36)$$

Loop stability requires that

$$C_1 + C_2 > \frac{\pi I_p K_{\text{VCO}}}{2M \omega_{\text{in}}^2} = C_{\text{stable}} \quad (37)$$

as if C_1 itself were raised by an amount equal to C_2 . For example, if R_1 is very small, then the loop filter can be approximated by $C_1 + C_2$, necessitating this condition.

Practical designs may lie somewhere between the above extreme cases, requiring numerical manipulation of (32). As an example, we return to the design in Section V with $\omega_{\text{in}} = 2\pi \times (125 \text{ MHz})$, $K_{\text{VCO}} = 2\pi \times (1.5 \text{ GHz/V})$, $M = 8$, and $I_p = 0.1 \text{ mA}$, and study the effect of C_2 on the phase margin. Plotted in Fig. 16 are a family of curves versus C_2/C_1 , obtained by calculating the real and imaginary parts of (32) and hence the phase margin. Also shown are the counterparts predicted by the LTI model. Our LTV model reveals that the loop becomes unstable if $C_1 = 0.4 \text{ pF}$ and C_2 reaches approximately $C_1/300$, whereas the LTI model implies a phase margin of about 45° . The discrepancy between the two models persists for a wide range of C_1 and C_2/C_1 .

VIII. CONCLUSION

In this paper, we have proposed both a small-signal analysis and a large-signal view of the stability in charge-pump phase-locked loops. We observe that the translational nature of the loop creates overlap between replica transfer functions, thereby degrading the stability. A closed-loop harmonic balance analysis yields a minimum required value for the main capacitor in the loop filter. It is also shown that the loop bandwidth can approach half of the input frequency while maintaining stability.

APPENDIX A

LOOP TRANSMISSION CALCULATION

Our analysis proceeds as follows. We wish to determine the closed-loop transfer function from the main input to the charge pump output and therefrom the loop transmission. For simplicity, we apply $V_{in}(t) = V_0 \cos(\omega_{in}t + 2\alpha \cos \omega_m t)$ so that the sidebands have a magnitude of α with respect to the carrier. We also assume that the sidebands in I_{cp} in Fig. 6 have a magnitude of β . Each sideband in I_{cp} is multiplied by $Z_{LCPF}(j\omega)$ to yield V_{cont} , e.g., the sideband at $n f_{in} + f_m$ emerges as $\beta Z_{LCPF}[j(n\omega_{in} + \omega_m)]$. Next, we multiply this result by the VCO/divider transfer function, obtaining $\beta Z_{LCPF}[j(n\omega_{in} + \omega_m)] \cdot K_{VCO}/[j(n\omega_{in} + \omega_m)] \cdot 1/M$ for V_{div} .

We must now determine how the above feedback components land around f_{in} after impulse sampling and charge pump operation. For example, to generate the sideband located at $f_{in} + f_m$, we must consider the following infinite series:

$$\begin{aligned} V_{div}(\omega) \propto & \frac{Z_{LCPF}[j(\omega_m)]}{j(\omega_m)} \delta(\omega - \omega_m) \\ & + \frac{Z_{LCPF}[j(\omega_{in} + \omega_m)]}{j(\omega_{in} + \omega_m)} \delta(\omega - \omega_{in} - \omega_m) \\ & + \frac{Z_{LCPF}[j(2\omega_{in} + \omega_m)]}{j(2\omega_{in} + \omega_m)} \delta(\omega - 2\omega_{in} - \omega_m) \\ & + \frac{Z_{LCPF}[j(3\omega_{in} + \omega_m)]}{j(3\omega_{in} + \omega_m)} \delta(\omega - 3\omega_{in} - \omega_m) + \dots \end{aligned} \quad (38)$$

The right hand side must be multiplied by $\beta K_{VCO}/M$ to yield V_{div} . Fig. 17 illustrates how this series arises from the shaped feedback spectrum. Of course, before reaching the charge pump, these terms must be subtracted from the input sidebands at $f_{in} \pm f_m$. The overall feedback equation thus emerges as

$$\begin{aligned} I_{cp}|_{f_{in}+f_m} = & \alpha \frac{I_p}{2\pi} - \frac{\beta K_{VCO} I_p Z_{LCPF}[j(\omega_{in} + \omega_m)]}{2\pi M j(\omega_{in} + \omega_m)} \\ & - \frac{\beta K_{VCO} I_p Z_{LCPF}[j(2\omega_{in} + \omega_m)]}{2\pi M j(2\omega_{in} + \omega_m)} \\ & - \frac{\beta K_{VCO} I_p Z_{LCPF}[j(3\omega_{in} + \omega_m)]}{2\pi M j(3\omega_{in} + \omega_m)} - \dots \end{aligned} \quad (39)$$

Equating this magnitude to β , we have

$$\frac{\beta}{\alpha} = \frac{\frac{I_p}{2\pi}}{1 + \frac{I_p K_{VCO}}{2\pi M} \sum_{n=-\infty}^{\infty} \frac{Z_{LCPF}[j(n\omega_{in} + \omega_m)]}{j(n\omega_{in} + \omega_m)}}. \quad (40)$$

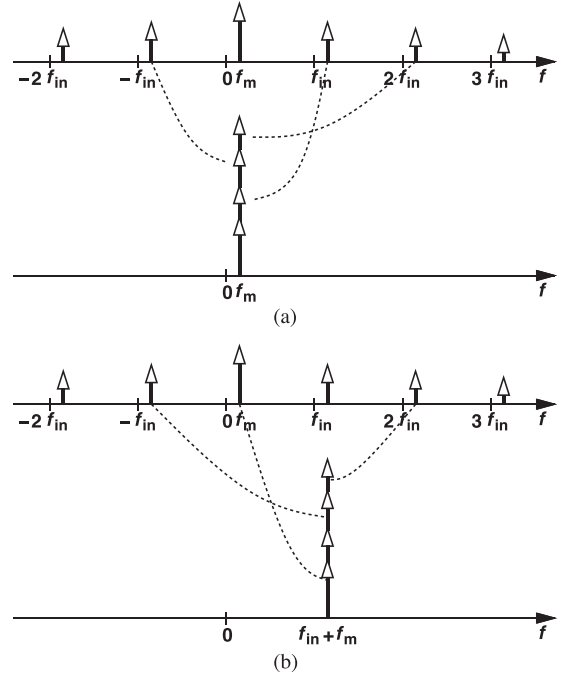


Fig. 17. Folding of all harmonics to (a) f_m , and (b) $f_{in} + f_m$.

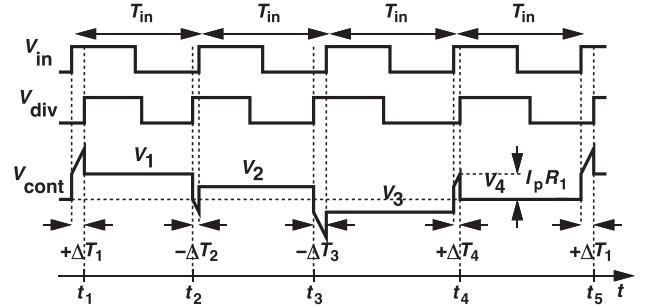


Fig. 18. Oscillatory behavior for general $f_{in}/4$ mode.

This is the closed-loop transfer function from the input phase to the charge pump output current. The loop transmission, $T(j\omega)$, is therefore given by

$$T(j\omega) = \frac{I_p K_{VCO}}{2\pi M} \sum_{n=-\infty}^{\infty} \frac{Z_{LCPF}[j(n\omega_{in} + \omega)]}{j(n\omega_{in} + \omega)}. \quad (41)$$

Note that ω_m is replaced with ω because this result applies to any input phase modulation at a rate of ω .

APPENDIX B

 $f_{in}/4$ -MODE OSCILLATION

In this appendix, we study the $f_{in}/4$ -mode oscillation. Fig. 18 sketches the $f_{in}/4$ mode with arbitrary ΔT 's and voltages. Based on integration over V_{div} periods, we write

$$\frac{K_{VCO} V_1 (T_{in} - \Delta T_1 - \Delta T_2)}{M} = 2\pi \quad (42)$$

$$\frac{K_{VCO}}{M} \left[V_2 (T_{in} - \Delta T_3) + \left(\frac{V_1 + V_2}{2} - I_p R_1 \right) \Delta T_2 \right] = 2\pi. \quad (43)$$

$$\frac{K_{VCO}}{M} \left[V_3 T_{in} + \left(\frac{V_2 + V_3}{2} - I_p R_1 \right) \Delta T_3 \right] + \frac{K_{VCO}}{M} \left[\left(\frac{V_3 + V_4}{2} + I_p R_1 \right) \Delta T_4 \right] = 2\pi. \quad (44)$$

$$\frac{K_{VCO}}{M} \left[V_4 (T_{in} - \Delta T_4) + \left(\frac{V_4 + V_1}{2} + I_p R_1 \right) \Delta T_1 \right] = 2\pi. \quad (45)$$

We also have $V_1 - V_2 = I_p \Delta T_2 / C_1$, $V_2 - V_3 = I_p \Delta T_3 / C_1$, $V_4 - V_3 = I_p \Delta T_4 / C_1$, $V_1 - V_4 = I_p \Delta T_1 / C_1$. These equations do not lend themselves to a closed-form solution, but they can be solved for a given design.

Unlike the $f_{in}/2$ and $f_{in}/3$ modes, the $f_{in}/4$ oscillation generally depends on the value of R_1 . It is possible to predict certain trends from the $f_{in}/4$ mode equations. We first note that the above $V_j - V_k$ equations yield $\Delta T_1 + \Delta T_4 = \Delta T_2 + \Delta T_3$.

Now suppose we allow R_1 to become arbitrarily large. We can prove that $\Delta T_1 \rightarrow 0$, $\Delta T_2 \rightarrow 0$, $\Delta T_4 - \Delta T_3 \rightarrow 0$. If both ΔT_1 and ΔT_2 are equal to zero, it means that V_{div} and V_{in} coincide for one period and there is no reason for the PLL to go out of lock. This analysis suggests that a sufficiently large R_1 suppresses the $f_{in}/4$ mode.

REFERENCES

- [1] A. B. Grebene, "The monolithic phase-locked loop—A versatile building block," *IEEE Spectrum*, vol. 8, no. 3, pp. 38–49, Mar. 1971.
- [2] D. Y. Abramovitch, "Lyapunov redesign of analog phase-lock loops," *IEEE Trans. Commun.*, vol. 38, no. 12, pp. 2197–2202, Dec. 1990.
- [3] N. V. Kuznetsov *et al.*, "Limitations of the classical phase-locked loop analysis," in *Proc. IEEE Int. Symp. Circuits Syst. (ISCAS)*, May 2015, pp. 533–536.
- [4] G. A. Leonov *et al.*, "Hold-in, pull-in, and lock-in ranges of PLL circuits: rigorous mathematical definitions and limitations of classical theory," *IEEE Trans. Circuits Syst. I, Reg. Papers*, vol. 62, no. 10, pp. 2454–2464, Oct. 2015.
- [5] R. E. Best *et al.*, "A short survey on nonlinear models of the classic costas loop: rigorous derivation and limitations of the classic analysis," in *Proc. Amer. Control Conf. (ACC)*, Jul. 2015, pp. 1296–1302.
- [6] J. Kudrewicz and S. Wasowicz, *Equations of Phase-Locked Loops: Dynamics on Circle, Torus and Cylinder*. Singapore: World Sci., 2007.
- [7] A. K. Belyaev, H. Irshik, and M. Krommer, *Mechanics and Model-Based Control of Advanced Engineering Systems*, Eds. New York, NY, USA: Springer, 2014.
- [8] N. I. Margaris, *Theory of the Non-Linear Analog Phase Locked Loop*. Berlin/Heidelberg, Germany: Springer-Verlag, 2004.
- [9] S. C. Gupta, "Phase-locked loops," *Proc. IEEE*, vol. 63, no. 2, pp. 291–306, Feb. 1975.
- [10] J. P. Hein and J. W. Scott, "Z-domain model for discrete-time PLLs," *IEEE Trans. Circuits Syst.*, vol. 35, no. 11, pp. 1393–1400, Nov. 1988.
- [11] S. Barab and A. L. McBride, "Uniform sampling analysis of a hybrid phase-locked loop with a sample-and-hold phase detector," *IEEE Trans. Aerosp. Electron. Syst.*, vol. AES-11, no. 2, pp. 210–216, Mar. 1975.
- [12] G. Kolumban, "Frequency domain analysis of sampling phase-locked loops," in *Proc. IEEE Int. Symp. Circuits Syst. (ISCAS)*, Jun. 1988, pp. 611–614.
- [13] J. A. Crawford, *Advanced Phase-Lock Techniques*. Norwood, MA, USA: Artech House, 2008.
- [14] F. Gardner, "Charge-pump phase-lock loops," *IEEE Trans. Commun.*, vol. COM-28, no. 11, pp. 1849–1858, Nov. 1980.
- [15] F. Gardner, *Phase-Lock Techniques*, 3rd ed. New York: Wiley, 2005.
- [16] A. Sklorz, "On charge-pump phase-locked loops modelling," in *Proc. IEEE Int. Symp. Circuits Syst. (ISCAS)*, Jun. 1988, pp. 643–646.
- [17] J. Lu *et al.*, "Discrete z-domain analysis of high order phase locked loops," in *Proc. IEEE Int. Symp. Circuits Syst.*, May 2001, pp. 260–263.
- [18] P. Vanasche, G. Gielen, and W. Sansen, "Time-varying, frequency-domain modeling and analysis of phase-locked loops with sampling phase-frequency detectors," in *Proc. Design, Autom., Test Eur. Conf. Exhib.*, 2003, pp. 238–243.
- [19] Z. Wang, "An analysis of charge-pump phase-locked loops," *IEEE Trans. Circuits Syst. I, Reg. Papers*, vol. 52, no. 10, pp. 2128–2138, Oct. 2005.
- [20] J. Rogers, C. Plett, and F. Dai, *Integrated Circuit Design for High-Speed Frequency Synthesis*. Norwood, MA, USA: Artech House, 2006.
- [21] P. K. Hanumolu *et al.*, "Analysis of charge-pump phase-locked loops," *IEEE Trans. Circuits Syst. I, Reg. Papers*, vol. 51, no. 9, pp. 1665–1674, Sep. 2004.
- [22] S. Miyazawa *et al.*, "A BiCMOS PLL-based data separator circuit with high stability and accuracy," *IEEE J. Solid-State Circuits*, vol. 26, no. 2, pp. 116–121, Feb. 1991.
- [23] I. I. Novof *et al.*, "Fully integrated CMOS phase-locked loop with 15 to 240 MHz locking range and ± 50 ps jitter," *IEEE J. Solid-State Circuits*, vol. 30, no. 11, pp. 1259–1266, Nov. 1995.



Aliakbar Homayoun (S'08–M'14) received the B.S. and M.S. degrees from Sharif University of Technology, Tehran, Iran, in 2006 and 2009, and the Ph.D. degree from the University of California, Los Angeles (UCLA), CA, USA, in 2013, all in electronics engineering. Following his Ph.D., he held a postdoctoral scholar position in the Communication Circuits Laboratory at UCLA. He has been with Corporate R&D at Qualcomm, San Diego, CA, USA, since April 2014. His research interest includes analog, RF, and millimeter-wave integrated circuit design for wireless transceivers and frequency synthesizers.



Behzad Razavi (S'87–M'90–SM'00–F'03) received the B.S.E.E. degree from Sharif University of Technology, Tehran, Iran, in 1985 and the M.S.E.E. and Ph.D.E.E. degrees from Stanford University, Stanford, CA, USA, in 1988 and 1992, respectively.

He was with AT&T Bell Laboratories and Hewlett-Packard Laboratories until 1996. Since 1996, he has been Associate Professor and subsequently Professor of Electrical Engineering at University of California, Los Angeles, CA, USA. He was an Adjunct Professor at Princeton University,

Princeton, NJ, USA, from 1992 to 1994, and at Stanford University in 1995. His current research includes wireless transceivers, frequency synthesizers, phase-locking and clock recovery for high-speed data communications, and data converters.

Prof. Razavi served on the Technical Program Committees of the International Solid-State Circuits Conference (ISSCC) from 1993 to 2002 and VLSI Circuits Symposium from 1998 to 2002. He has also served as Guest Editor and Associate Editor of the IEEE JOURNAL OF SOLID-STATE CIRCUITS, IEEE TRANSACTIONS ON CIRCUITS AND SYSTEMS, and *International Journal of High Speed Electronics*. Prof. Razavi received the Beatrice Winner Award for Editorial Excellence at the 1994 ISSCC, the best paper award at the 1994 European Solid-State Circuits Conference, the best panel award at the 1995 and 1997 ISSCC, the TRW Innovative Teaching Award in 1997, the best paper award at the IEEE Custom Integrated Circuits Conference in 1998, and the McGraw-Hill First Edition of the Year Award in 2001. He was the co-recipient of both the Jack Kilby Outstanding Student Paper Award and the Beatrice Winner Award for Editorial Excellence at the 2001 ISSCC. He received the Lockheed Martin Excellence in Teaching Award in 2006, the UCLA Faculty Senate Teaching Award in 2007, and the CICC Best Invited Paper Award in 2009. He was also recognized as one of the top 10 authors in the 50-year history of ISSCC. He received the 2012 Donald Pederson Award in Solid-State Circuits. He was also the recipient of the American Society for Engineering Education PSW Teaching Award in 2014. Prof. Razavi has served as an IEEE Distinguished Lecturer and is a Fellow of IEEE. He is the author of *Principles of Data Conversion System Design* (IEEE Press, 1995), *RF Microelectronics* (Prentice Hall, 1998, 2012) (translated to Chinese, Japanese, and Korean), *Design of Analog CMOS Integrated Circuits* (McGraw-Hill, 2001) (translated to Chinese, Japanese, and Korean), *Design of Integrated Circuits for Optical Communications* (McGraw-Hill, 2003, Wiley, 2012), and *Fundamentals of Microelectronics* (Wiley, 2006) (translated to Korean and Portuguese), and the editor of *Monolithic Phase-Locked Loops and Clock Recovery Circuits* (IEEE Press, 1996), and *Phase-Locking in High-Performance Systems* (IEEE Press, 2003).